

NeuralRemaster: Phase-Preserving Diffusion for Structure-Aligned Generation

Yu Zeng¹, Charles Ochoa¹, Mingyuan Zhou², Vishal M. Patel³,
Vitor Guizilini¹, and Rowan McAllister¹

¹ Toyota Research Institute

² University of Texas, Austin

³ Johns Hopkins University

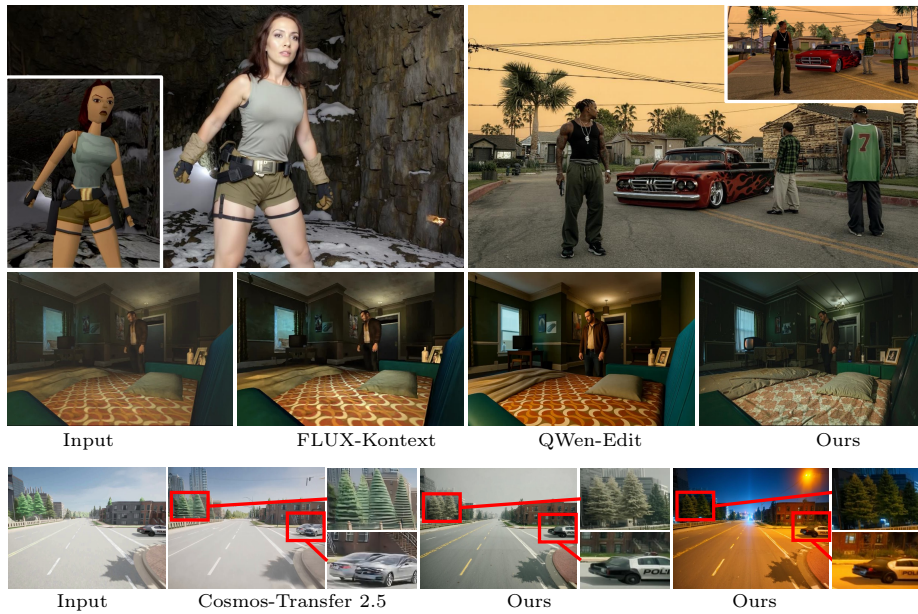


Fig. 1: We present Phase-Preserving Diffusion (ϕ -PD), a model-agnostic reformulation of the diffusion process that preserves an image’s phase while randomizing its magnitude, enabling structure-aligned generation with **no architectural changes or additional parameters**.

Abstract. Standard diffusion corrupts data using Gaussian noise whose Fourier coefficients have random magnitudes and random phases. While effective for unconditional or text-to-image generation, corrupting phase components destroys spatial structure, making it ill-suited for tasks requiring geometric consistency, such as re-rendering, simulation enhancement, and image-to-image translation. We introduce Phase-Preserving Diffusion (ϕ -PD), a model-agnostic reformulation of the diffusion process that preserves input phase while randomizing magnitude, enabling structure-aligned generation without architectural changes or additional

parameters. We further propose Frequency-Selective Structured (FSS) noise, which provides continuous control over structural rigidity via a single frequency-cutoff parameter. ϕ -PD adds no inference-time cost and is compatible with any diffusion model for images or videos. Across photo-realistic and stylized re-rendering, as well as sim-to-real enhancement for driving planners, ϕ -PD produces controllable, spatially aligned results. When applied to the CARLA simulator, ϕ -PD significantly improves sim-to-real planner transfer performance. The method is complementary to existing conditioning approaches and broadly applicable to image-to-image and video-to-video generation. Videos, additional examples, and code are available on our [project page](#).

1 Introduction

Recent advances in diffusion models have revolutionized image generation, achieving high-fidelity results for unconditional or text-conditioned synthesis. Yet many practical applications do not require generating a scene from scratch. Instead, they operate within an image-to-image setting where the spatial layout, such as object boundaries, geometry and scene structures, should remain fixed while the appearance is modified. Examples include neural rendering, stylization, and sim-to-real transfer for autonomous driving or robotics simulation. We refer to this broad class of problems as **structure-aligned generation**.

Although these tasks are conceptually easier than generating from scratch, existing solutions are unnecessarily complex. Methods such as ControlNet [43], T2I-Adapter [21], and related variants attach auxiliary branches to inject structural input into the model. While effective, this introduces additional parameters and computational cost, paradoxically making structure-aligned generation harder than it should be.

We argue that this inefficiency stems not from the network architecture, but from the diffusion process itself. The forward diffusion process injects Gaussian noise, which destroys both the magnitude and phase components in the frequency domain. Classical signal processing [23, 31, 38], however, tells us that phase encodes structure while magnitude encodes texture. Destroying the phase means destroying the very spatial coherence that structure-aligned generation depends on, forcing the model to reconstruct structure from scratch.

Motivated by this insight, we propose Phase-Preserving Diffusion (ϕ -PD). Instead of corrupting data with Gaussian noise, ϕ -PD constructs *structured noise* whose magnitude matches that of Gaussian noise while preserving the input phase. This naturally maintains spatial alignment throughout sampling (Figure 1) with **no architectural modification, no extra parameters** (Figure 2), and is compatible with any DDPM or flow-matching model for images or videos.

To provide controllable levels of structural rigidity, we further introduce **Frequency-Selective Structured (FSS) noise**, which interpolates between input phase and pure Gaussian noise via a single cutoff parameter (Figure 4). This allows us to control the trade-off between strict alignment and creative flexibility.

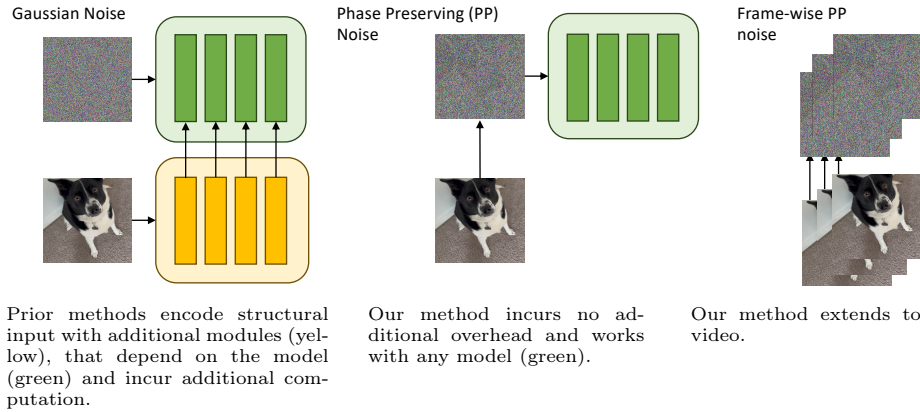


Fig. 2: Unlike prior approaches that modify architectures and add overhead, ϕ -PD preserves structure via phase consistency, remaining lightweight and model-agnostic, reflecting that image-conditioned generation should be simpler, not harder.

We evaluate ϕ -PD across photorealistic re-rendering, stylized re-rendering and simulation enhancement for embodied-AI agents. ϕ -PD consistently maintains geometry alignment while producing high-quality visual outputs, outperforming prior methods across both quantitative and qualitative metrics. When used to enhance CARLA simulations, ϕ -PD improves planner transfer to the Waymo Open Dataset by 50%, substantially narrowing the sim-to-real gap. In summary, our contributions include:

- **Phase-preserving diffusion process:** A diffusion process that preserves phase while randomizing magnitude in frequency domain, maintaining spatial structure without architectural changes.
- **Frequency-selective structured noise:** A single-parameter mechanism that enables continuous control over structural alignment rigidity.
- **Unified and efficient framework** applicable to both images and videos, compatible with DDPMs and flow-matching, and requires no inference-time overhead.

2 Related Work

Diffusion Models. Diffusion models have become a dominant paradigm for generative modeling, capable of representing complex data distributions with remarkable fidelity [11, 16]. They progressively corrupt data into Gaussian noise through a forward diffusion process, then learn to invert this process via iterative denoising. This framework has demonstrated state-of-the-art performance across diverse domains, including image, video, and audio generation [3, 4, 12, 17, 25, 29, 32], as well as reinforcement learning [14, 26, 37] and robotics [1, 5, 36].

Frequency-Domain Manipulation for Diffusion. Recent work has explored frequency domain operations for diffusion models. [7] argues that diffusion models of images perform approximate autoregression in the frequency domain. [9] shows that the standard diffusion forward process corrupts high-frequency components faster than low-frequency ones, and introduces an alternate process that corrupts all frequencies at the same rate. [41] shows that modifying the UNet frequency domain features significantly improves the generating quality for image or video generation. FreeDiff [39] introduces a fine-tuning free approach for image editing that employs progressive frequency truncation to refine the guidance of diffusion models. [45] proposes a training-free style transfer method that modulates the intermediate samples with the image phase. [27] proposed to use a frequency-dependent moving average during sampling. [2] proposes a training-free approach for image inpainting that optimizes the initial seed noise in the spectral domain.

Structure-Aligned Generation with Diffusion. Most existing methods achieve structure-aligned generation by modifying the network architecture and introducing additional adaptation components. ControlNet [43] copies the entire UNet encoder into a trainable encoder branch, which adds significant computation overhead. T2I-Adapter [21] reduces computation overhead using a lightweight adapter module but sacrifices control precision. Uni-ControlNet [46] enables simultaneous utilization of multiple local controls by training two adapters. Omni-Control [33] integrates image conditions into Diffusion Transformer (DiT) architectures with only 0.1% additional parameters by re-using the VAE and transformer blocks of the base model. ControlNeXt [24] uses a lightweight convolutional module to inject control signals, and directly finetune selective parameters of the base model to reduce training costs and latency increase. SCedit [15] proposes an efficient finetuning framework that edits skip connections using a lightweight module. NanoControl [13] aims to achieve efficient control with a LoRA-style control module. The above methods all rely on an additional module to incorporate the control signal, though some are more lightweight than others. CosmosTransfer [22] achieves multi-modal control by combining multiple ControlNet branches, demonstrating promising applications on physical tasks; however, multiple branches introduce significant computation overhead. In contrast, ϕ -PD does not introduce any computation overhead or additional parameters while enabling universal spatial control.

Training-Free Guidance Methods. Recently, several training-free methods have been developed. [42] introduced FreeDoM, which leverages off-the-shelf pre-trained networks to construct time-independent energy functions that guide generation. [6] proposed ZestGuide for zero-shot spatial layout conditioning, utilizing implicit segmentation maps extracted from cross-attention layers to align generation with input masks. [20] presented FreeControl, a training-free approach that enforces structure guidance with the base model feature extracted from the control signal. Although these methods avoid training cost, they introduce additional overhead at test time, either an external model, DDIM inversion,

or multiple inferences of the base model. In contrast, ϕ -PD achieves spatial control without any additional inference time overhead.

3 Method

3.1 Frequency Domain Fundamentals

In the frequency domain, any image $I(x, y)$ can be represented through the 2D Fourier transform:

$$F(u, v) = \mathcal{F}\{I(x, y)\} = \sum_{x=0}^{W-1} \sum_{y=0}^{H-1} I(x, y) e^{-2\pi j(ux/W+vy/H)}, \quad (1)$$

where $F(u, v)$ is a complex-valued function that can be decomposed into magnitude and phase components:

$$F(u, v) = |F(u, v)| \cdot e^{j\phi(u, v)} = A(u, v) \cdot e^{j\phi(u, v)}. \quad (2)$$

Here, $A(u, v) = |F(u, v)|$ is the magnitude spectrum and $\phi(u, v)$ the phase spectrum. The inverse Fourier transform uses magnitude and phase to reconstruct the original image:

$$I(x, y) = \mathcal{F}^{-1}\{F(u, v)\} = \sum_{u=0}^{W-1} \sum_{v=0}^{H-1} F(u, v) e^{2\pi j(ux/W+vy/H)}. \quad (3)$$

Phase-Magnitude Separation in Signal Processing. Foundational work by Oppenheim [23] shows that phase primarily determines spatial structure, while magnitude largely controls texture statistics. Mixing phase and magnitude from different images produces reconstructions whose spatial layout follows the source of the phase, not magnitude (see Figure 3). This observation motivates our approach: if diffusion destroys phase, it destroys spatial geometry; if we preserve phase, we preserve structure.

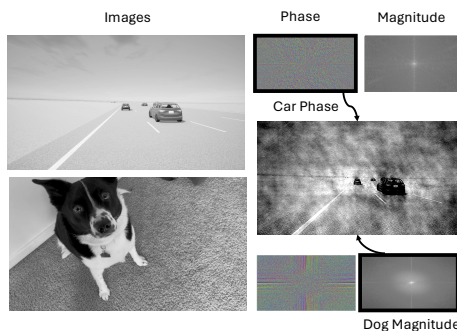


Fig. 3: Mixing phase and magnitude from two images. The mixture keeps the structure of the image where the phase is taken.

3.2 Phase-Preserving Diffusion

Standard diffusion corrupts data using Gaussian noise whose Fourier coefficients have random magnitudes and random phases. As a result, even early diffusion

steps erase spatial alignment. We propose a simple alternative: *preserve the input image’s phase and randomize the magnitude*, by using structured noise that shares the input phase.

Structured Noise Construction. Given an input image I , we compute its Fourier transform:

$$F_I = A_I \cdot e^{j\phi_I}. \quad (4)$$

We construct **phase-preserving noise** by pairing the input image phase with a random magnitude:

$$F_{\hat{\epsilon}} = A_{\epsilon} \cdot e^{j\phi_I}, \quad (5)$$

and invert it:

$$\hat{\epsilon} = \mathcal{F}^{-1}\{F_{\hat{\epsilon}}\}, \quad (6)$$

where the random magnitude A_{ϵ} can be obtained from the Fourier transform of Gaussian noise:

$$A_{\epsilon} = |\mathcal{F}\{\epsilon\}|, \quad \epsilon \sim \mathcal{N}(0, I). \quad (7)$$

Alternatively, A_{ϵ} can be sampled from a scaled Rayleigh distribution [10]:

$$A_{\epsilon} = \sqrt{-N \ln U}, \quad U \sim \text{Uniform}(0, 1), \quad (8)$$

where $N = H \times W$, matching the magnitude statistics of the DFT of unit-variance Gaussian noise.

This structured noise is used in place of Gaussian noise in forward diffusion for training. It injects randomness while maintaining the phase of the input. At test time, we achieve structure-aligned generation by starting sampling from structured noise constructed with input image phase.

Frequency Selective Structured (FSS) Noise. In practice, we often want to control to what extent we keep the structure from the input image. Some tasks require strict structure preservation, while others benefit from partial freedom to reinterpret the scene. To provide this control, we introduce Frequency Selective Structured (FSS) noise, which only keep the image within a radius r and use the phase from the noise for the remainder. We define a smooth frequency mask $M(u, v)$ based on the cutoff radius r :

$$M(u, v) = \begin{cases} 1 & \text{if } \sqrt{u^2 + v^2} \leq r \\ \exp\left(-\frac{(\sqrt{u^2 + v^2} - r)^2}{2\sigma^2}\right) & \text{if } \sqrt{u^2 + v^2} > r \end{cases} \quad (9)$$

where (u, v) are centered frequency coordinates with the DC component at the origin, and r is specified in pixels relative to the frequency grid of size $W \times H$. In practice, we use `fftshift` to center the spectrum before applying the mask.

The FSS noise $\hat{\epsilon}$ is the combination of image phase and noise phase using the mask:

$$F_{\hat{\epsilon}} = A_{\epsilon} \cdot e^{j\phi_I \odot M + j\phi_{\epsilon} \odot (1-M)}, \quad (10)$$



Fig. 4: Frequency Selective Structured (FSS) Noise with increasing cutoff radius r .

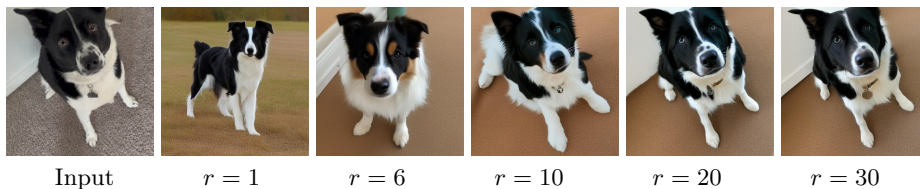


Fig. 5: Image generated with the same noise and different cutoff radius r . Results are based on SD1.5.

where \odot represents element-wise multiplication. We can sample phase ϕ_ϵ as the Fourier transform of Gaussian noise:

$$\begin{aligned} \epsilon &\sim \mathcal{N}(0, 1), \\ \phi_\epsilon &= \arg(\mathcal{F}\{\epsilon\}) \sim \text{Uniform}(-\pi, \pi). \end{aligned} \quad (11)$$

When the mask is all zero, we take a random phase for all frequencies, then this FFS noise becomes Gaussian noise and ϕ -PD becomes standard diffusion. Figure 4 visualizes FFS noise with different cutoff radius r . We can see that the noise becomes increasingly more structured with increasing r . Figure 5 shows images generated from the same input with different cutoff radius where the generated image aligns more tightly to the input with larger r .

3.3 Training Objective

ϕ -PD does not depend on model architecture or diffusion formulation. In the experiment section, we demonstrate integration both DDPM and Flow Matching, without modifying their architectures or loss functions.

The flow matching objective learns a vector field that transports the structured noise distribution to the target image distribution. During training, given a target image I and a structured noise $\hat{\epsilon}$, and a timestep $t \in [0, 1]$, an intermediate image x_t is obtained using a linear combination between I and $\hat{\epsilon}$ following Rectified Flows [19]:

$$x_t = t \hat{\epsilon} + (1 - t) I. \quad (12)$$

The ground-truth velocity is

$$v_t = \frac{dx_t}{dt} = \hat{\epsilon} - I. \quad (13)$$

With this ground-truth, we can then train the model by minimizing the mean squared error between the model output and the ground-truth:

$$\mathcal{L} = \mathbb{E}_{I, \hat{\epsilon}, t} \|u(x_t, t; \theta) - v_t\|_2^2. \quad (14)$$

In the Fourier domain, when using full phase-preservation, the velocity becomes

$$F_{v_t} = (A_{\hat{\epsilon}} - A_I) e^{j\phi_I} \quad (15)$$

which has phase ϕ_I or $\phi_I + \pi$, preserving structural alignment. With FSS noise, phase is preserved within the cutoff radius r , providing controllable alignment strength.

In DDPMs [11], data x_0 is gradually corrupted by Gaussian noise:

$$q(x_t | x_{t-1}) = \mathcal{N}(\sqrt{1 - \beta_t} x_{t-1}, \beta_t I). \quad (16)$$

The model learns the reverse process by predicting the added noise ϵ at each step using the loss

$$\mathcal{L}_{\text{DDPM}} = \mathbb{E}_{x_0, \epsilon, t} [\|\epsilon - \epsilon_\theta(x_t, t)\|_2^2], \quad (17)$$

where $x_t = \sqrt{\bar{\alpha}_t} x_0 + \sqrt{1 - \bar{\alpha}_t} \epsilon$ and $\bar{\alpha}_t = \prod_{s=1}^t (1 - \beta_s)$.

In our formulation, we replace the Gaussian noise ϵ with structured noise $\hat{\epsilon}$ that preserves the input phase:

$$x_t = \sqrt{\bar{\alpha}_t} x_0 + \sqrt{1 - \bar{\alpha}_t} \hat{\epsilon}. \quad (18)$$

The training objective follows the same form,

$$\mathcal{L}_{\phi\text{-PD}} = \mathbb{E}_{x_0, \hat{\epsilon}, t} [\|\hat{\epsilon} - \epsilon_\theta(x_t, t)\|_2^2], \quad (19)$$

but the expectation is now over structured noise $\hat{\epsilon}$ rather than Gaussian noise ϵ . Although $\hat{\epsilon}$ is non-Gaussian and formally violates standard DDPM assumptions, we observe high-quality, structure-aligned outputs using standard samplers after finetuning with this objective.

3.4 Extension to Videos

ϕ -PD extends to video by constructing phase-preserving noise frame-by-frame. For a video $\{I_1, I_2, \dots, I_T\}$, we construct structured noise for each frame and concatenate along the time dimension. Since current video diffusion models produce lower-fidelity individual frames than image models, we adopt a two-stage pipeline: generating the initial frame with image-based ϕ -PD, then extending temporally with first-frame-conditioned video ϕ -PD. No architectural changes are required.



Fig. 6: Results on UnrealCV compared to FLUX-Kontext and QWenEdit.

4 Experiments

We evaluate ϕ -PD across three settings: photorealistic re-rendering, stylized re-rendering, and simulation enhancement for autonomous driving, comparing against state-of-the-art methods. To demonstrate its broad applicability, we implement ϕ -PD on three representative diffusion models: SD 1.5, FLUX-dev, and WAN 2.2 14B, which vary in size, formulation, and modality, covering both image and video generation. Please refer to the supplementary materials for additional results and code.

During training, we use real images: construct structured noise from the image’s phase, corrupt the image, and train the model to denoise. At inference, ϕ -PD supports two inference modes. (1) Structured SDEdit: add structured noise to the source image at some noise level t , then denoise. (2) From noise: denoise from pure structured noise without any pixel contribution from the source; structure is encoded entirely in the phase. Mode (1) generally yields stronger structural alignment; mode (2) offers more flexibility with larger appearance changes.

4.1 Implementation Details

Datasets **UnrealCV**⁴ is an open-source tool that includes multiple assets. We created a diverse test set consisting of around 5,000 images across all available assets, for a total of around 200 scenes. Figure 6 shows examples from this test set. This dataset covers a diverse range of scenes, including outdoor and indoor, city and natural etc, with geometry diversity while lacking photorealism. This dataset evaluates photorealistic enhancement and structure preservation.

⁴ <https://github.com/unrealcv/unrealcv>

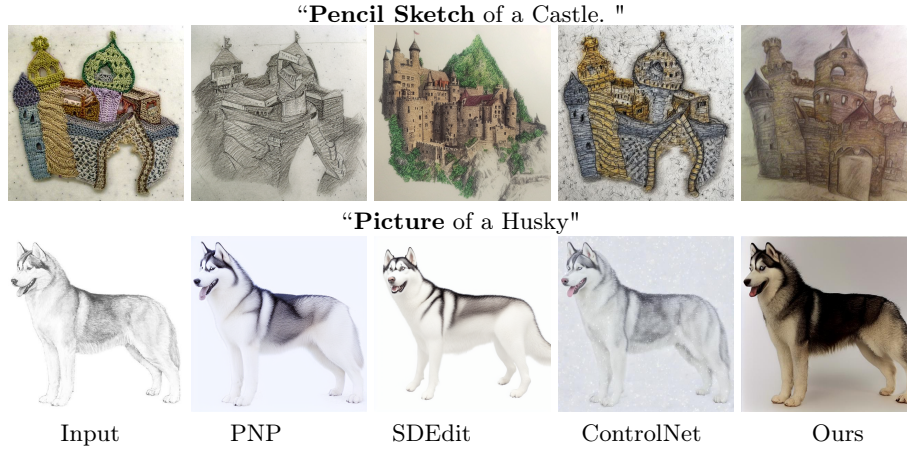


Fig. 7: Stylized re-rendering results.

ImageNetR is a test set proposed by [35], including 29 images of various objects and styles. While the original dataset provides prompts, these are generic image editing prompts. Since our work primarily focuses on re-rendering, we keep the editing prompts with style hints in the original dataset and added additional style prompts, resulting in a total of 8 prompts for each image. This benchmark assesses stylized re-rendering and structure preservation.

CARLA is an open-source driving simulator [8]. We collect 5.5 hours of driving videos from *CARLA Town 4* using the simulator’s default autopilot. We then split the videos into 25 second clips and annotate a caption for each clip. For simulation enhancement, we use these captions combined with the style hint “A photorealistic video of driving”. We evaluate the effectiveness of sim-to-real transfer by testing the CARLA-trained planner on Waymo’s WOD-E2E [40] validation set.

Model architecture We integrate ϕ -PD into: SD 1.5 (image DDPM), FLUX-dev (image flow matching), and Wan2.2-14B (video flow matching). We either fully finetune or LoRA-finetune each model using phase-preserving noise; no architectural changes are introduced. Notably, this finetuning is highly efficient: adapting the Wan2.2-14B video model with LoRA required only a single GPU while still yielding high-quality results, further demonstrating the lightweight nature of ϕ -PD. To evaluate structure alignment, we compute LPIPS [44] between the input and output pairs, as well as the error between their depth map using metrics SSIM (Structural Similarity Index Measure) and ABSREL (Absolute Relative error). To evaluate text prompt alignment, we compute CLIP [28] similarity between the generated images and the input text prompt.

Training and Inference Details We start from the officially released checkpoints of SD 1.5 [30], FLUX-dev [18], and Wan2.2-14B [34], and finetune each

Table 1: Quantitative evaluation results for photorealistic re-rendering on UnrealCV.

Method	Prompt Align.	Structure Alignment		
	CLIP \uparrow	LPIPS \downarrow	SSIM \uparrow	ABSREL \downarrow
ControlNet-Tile	0.3018	0.5831	0.6804	0.9484
PNP	0.2978	0.4076	0.6993	0.8870
FBSDiff	0.3255	0.3558	0.6792	0.9362
SDEdit	0.2989	0.4540	0.6754	0.8932
Ours	0.3212	0.2397	0.7481	0.5589

model with phase-preserving noise. For SD 1.5, we experiment with both full finetuning and LoRA finetuning, while for FLUX-dev and Wan2.2-14B we use LoRA finetuning due to computational constraints. At inference time, for Wan2.2-14B we adopt the 4-step LoRA from LightX2V⁵ and apply it directly on top of our finetuned LoRA weights to accelerate sampling. FLUX and SD 1.5-based models are trained on PhotoConceptBucket dataset⁶; WAN2.2-14B based models are trained on OpenSoraPlan dataset⁷.

We LoRA finetune Wan2.2-14B for 1,200 iterations and FLUX-dev for 10,000 iterations, while SD 1.5 is fully finetuned for 140,000 iterations. Each training run takes approximately 48 hours on an NVIDIA A100 GPU.

For each training iteration, we sample a cutoff radius r from an exponential distribution and add a constant offset r_0 to ensure a minimum amount of phase information is always preserved:

$$r = r_0 + r', \quad r' \sim \text{Exp}(\lambda), \quad (20)$$

where $\lambda > 0$ is the rate parameter of the exponential distribution and r_0 controls the minimum cutoff. In our experiments, we set $\lambda = 0.1$ empirically. We set the transition bandwidth parameter $\sigma = 2$, which controls the smoothness of the frequency mask $M(u, v)$ around the cutoff radius r .

4.2 Results

Photorealistic Re-Rendering. Quantitative results on UnrealCV re-rendering are summarized in Table 1, where all methods are implemented using the SD 1.5-based models for fair quantitative comparison. We evaluate SDEdit with Gaussian noise (SDEdit) and structured noise (Ours) at identical noise levels ($t=0.5$). This comparison shows that, compared to Gaussian noise, structured noise consistently improves structure preservation (near 90% improvements on LPIPS) while maintaining text prompt alignment. Qualitative examples are shown in Figure 6, which compares our Flux-based model against stronger recent models

⁵ <https://huggingface.co/lightx2v/Wan2.2-Lightning>

⁶ <https://huggingface.co/datasets/bghira/photo-concept-bucket>

⁷ <https://huggingface.co/datasets/LanguageBind/Open-Sora-Plan-v1.1.0/tree/main>

Table 2: Quantitative evaluation for stylized re-rendering.

Method	Prompt Align.	Structure Alignment		
	CLIP \uparrow	LPIPS \downarrow	SSIM \uparrow	ABSREL \downarrow
ControlNet-Tile	0.3022	0.5849	0.7508	0.9085
PNP	0.2983	0.3029	0.7796	0.8816
FBSDiff	0.3091	0.3150	0.7562	0.9736
SDEdit	0.3011	0.3456	0.7588	0.9148
Ours	0.3017	0.2759	0.7842	0.8087

Table 3: Efficiency comparison in extra parameters and FLOPs relative to the base model as well as wall-clock time.

	ControlNet	SDEdit	PNP	FBSDiff	Ours
Extra Params	+50%	+0%	+0%	+0%	+0%
Extra FLOPs	+50%	+0%	+100%	+1100%	+0%
Time (s/image)	28.02	20.31	20.40	133.8	20.22

such as FLUX-Kontext, and Qwen-Edit. Across both settings, all methods improve photorealism-as reflected by higher AS scores than the input images while ϕ -PD achieves the highest photorealism and superior structure alignment. We observe that QWen-Edit produces visually high-quality results but often fails to maintain structural alignment with the input image; for example, in the first four cases, it enlarges the main subjects significantly. FLUX-Kontext aligns better with the input structure but provides only limited improvement in visual quality. Our method achieves both high visual fidelity and consistent structural alignment across frames.

Stylized Re-rendering. Results of stylized re-rendering are presented in Table 2, with representative examples shown in Figure 7. All models are based on SD 1.5. This task evaluates the model’s ability to alter appearance while preserving scene structure. As shown, ϕ -PD produces visually coherent stylizations that maintain object boundaries and spatial consistency, while prior methods often distort geometry or introduce texture misalignment. Quantitatively, ϕ -PD achieves similar prompt alignment and significantly higher structure alignment.

Simulation Enhancement. For this experiment, we generate 5.5 hours of demonstration driving videos from CARLA using its autopilot. Then we train an end2end planner on the re-rendered CARLA videos from each method using a ResNet backbone with a GRU to take temporal input and an MLP head to output a trajectory $\in \mathcal{R}^{16 \times 2}$ (4s predictions at 4Hz in XY space). As baseline, we also present the results from a purely CARLA-trained model. Open-

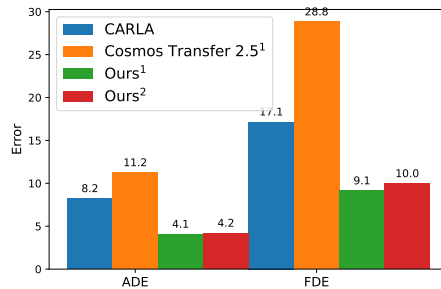
**Fig. 8:** Planner error on Waymo validation set. Lower is better. ¹zero-shot, ²finetuned on Waymo training set videos.



Fig. 9: Video re-rendering results on CARLA.

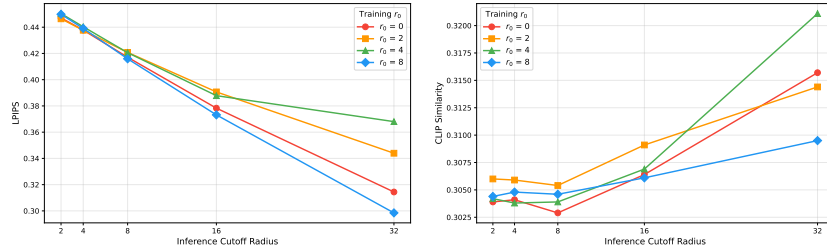


Fig. 10: LPIPS and CLIP scores with different r_0 and r .

loop imitation driving results are given in Figure 8. ϕ -PD boosts planner generalization by 50% in zero-shot setting, demonstrating that structure-preserving appearance enhancement significantly reduces the sim-to-real gap. Video examples in Figure 9 show that ϕ -PD maintains road boundaries, vehicle shapes, and spatial layout consistently across frames, whereas the compared method produces distorted trees and multi-object artifacts.

Efficiency Comparison. Table 3 compares the extra parameters and FLOPs relative to the base model, as well as the wall-clock time each method takes to process an image. ControlNet Tile adds 50% parameters and computation overhead (UNet + ControlNet model per step. PNP is $2 \times$ more expensive than the base model due to inversion and sampling, however achieves similar wall-clock time thanks to optimized implementation from diffuser. FBSDiff is extremely expensive ($12 \times$ base model FLOPs) due to 1000 inversion steps and 100 sampling steps. Our method does not introduce extra parameters or FLOPs.

5 Ablation Studies

5.1 Cutoff Radius

We ablate the choices of r_0 , the minimal cutoff radius at training time, and the inference-time cutoff radius r in this section. All ablation experiments are conducted using SD 1.5 with LoRA finetuning and evaluated on 1,000 randomly selected samples from the UnrealCV test set. Figure 10 shows how r_0 and r affects these metrics. Increasing the inference-time cutoff radius r significantly improves structural alignment: LPIPS drops from 0.44 – 0.45 to 0.30 – 0.38, while the change in text alignment is small: CLIP scores stay around 0.30 – 0.32. The minimal cutoff threshold r_0 during training influences the structural alignment with a large inference time cutoff radius r . It also affects performance across different inference-time radii r . A higher r_0 during training leads to better performance with higher r during inference, while a lower r_0 favors scenarios with smaller inference-time r .

5.2 Phase Preservation in Latent Space.

Classical results on phase-structure correspondence [23] were established in pixel space, while modern diffusion models operate in VAE latent space. We apply phase preservation directly to latents. While a complete theoretical analysis of how phase-structure relationships transfer through nonlinear encoders is beyond the scope of this work, we provide empirical validation in Figure 11.

We encode two images I_1 and I_2 into VAE latent representations z_1 and z_2 , then swap their Fourier magnitude and phase components. Combining the phase from z_1 with the magnitude from z_2 produces a decoded image that preserves the structure of I_1 (the dog’s silhouette), as shown in the top row. The bottom row shows the reverse combination which preserves the structure of I_2 (road, horizon, vehicles). This suggests that VAE latents, which are trained to preserve perceptually meaningful spatial structure, maintain sufficient phase-structure correspondence for our method to be effective.

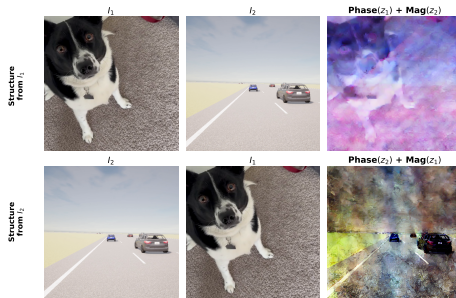


Fig. 11: Phase-structure correspondence in VAE latent space.

6 Conclusion

We introduced Phase-Preserving Diffusion (ϕ -PD), a simple yet effective reformulation of the diffusion process that replaces Gaussian noise with structured noise, preserving image phase while randomizing the magnitude in the

frequency domain. This simple change retains spatial alignment throughout sampling without modifying the architecture, altering training objectives, or introducing inference-time overhead. We also introduced Frequency-Selective Structured (FSS) noise, which provides continuous control over structural alignment rigidity through a single frequency cutoff parameter, making it broadly applicable to different applications.

Limitation. ϕ -PD assumes image-like inputs; modalities such as depth or normals may require a lightweight prior to produce an initial image representation.

Future work. ϕ -PD is orthogonal to existing conditioning or adapter methods and can be integrated with them for enhanced control. Future work includes extending ϕ -PD to tasks such as deblurring, relighting, super-resolution, and general image restoration.

References

1. Anurag Ajay, Yilun Du, Abhi Gupta, Joshua Tenenbaum, Tommi Jaakkola, and Pulkit Agrawal. Is conditional generative modeling all you need for decision-making? *arXiv preprint arXiv:2211.15657*, 2022. 3
2. Seungyeon Baek, Erqun Dong, Shadan Namazifard, Mark J Matthews, and Kwang Moo Yi. Sonic: Spectral optimization of noise for inpainting with consistency. *arXiv preprint arXiv:2511.19985*, 2025. 4
3. Yogesh Balaji, Seungjun Nah, Xun Huang, Arash Vahdat, Jiaming Song, Qinsheng Zhang, Karsten Kreis, Miika Aittala, Timo Aila, Samuli Laine, et al. eDiff-I: Text-to-image diffusion models with an ensemble of expert denoisers. *arXiv preprint arXiv:2211.01324*, 2022. 3
4. Haoxin Chen, Menghan Xia, Yingqing He, Yong Zhang, Xiaodong Cun, Shaoshu Yang, Jinbo Xing, Yaofang Liu, Qifeng Chen, Xintao Wang, et al. VideoCrafter1: Open diffusion models for high-quality video generation. *arXiv preprint arXiv:2310.19512*, 2023. 3
5. Cheng Chi, Siyuan Feng, Yilun Du, Zhenjia Xu, Eric Cousineau, Benjamin Burchfiel, and Shuran Song. Diffusion policy: Visuomotor policy learning via action diffusion. *arXiv preprint arXiv:2303.04137*, 2023. 3
6. Guillaume Couairon, Marlène Careil, Matthieu Cord, Stéphane Lathuilière, and Jakob Verbeek. Zero-shot spatial layout conditioning for text-to-image diffusion models. In *Proceedings of the IEEE/CVF International Conference on Computer Vision (ICCV)*, pages 2174–2183, October 2023. 4
7. Sander Dieleman. Diffusion is spectral autoregression. [urlhttps://sander.ai/2024/09/02/spectral-autoregression.html](https://sander.ai/2024/09/02/spectral-autoregression.html), September 2024. Accessed: 7 Dec 2025. 4
8. Alexey Dosovitskiy, German Ros, Felipe Codevilla, Antonio Lopez, and Vladlen Koltun. CARLA: An open urban driving simulator, 2017. 10
9. Fabian Falck, Teodora Pandeva, Kiarash Zahirnia, Rachel Lawrence, Richard Turner, Edward Meeds, Javier Zazo, and Sushrut Karmalkar. A fourier space perspective on diffusion models. *arXiv preprint arXiv:2505.11278*, 2025. 4
10. Joseph W. Goodman. *Statistical Optics*. Wiley, 2 edition, 2015. Section 2.9.3. 6
11. Jonathan Ho, Ajay Jain, and Pieter Abbeel. Denoising diffusion probabilistic models. *Advances in Neural Information Processing Systems*, 33:6840–6851, 2020. 3, 8

22. Jonathan Ho, Tim Salimans, Alexey Gritsenko, William Chan, Mohammad Norouzi, and David J Fleet. Video diffusion models. *Advances in Neural Information Processing Systems*, 35:8633–8646, 2022. [3](#)
23. Huang et al. NanoControl: A lightweight framework for precise and efficient control in diffusion transformer. *arXiv preprint arXiv:2508.10424*, 2024. [4](#)
24. Michael Janner, Yilun Du, Joshua B Tenenbaum, and Sergey Levine. Planning with diffusion for flexible behavior synthesis. *arXiv preprint arXiv:2205.09991*, 2022. [3](#)
25. Zeyinzi Jiang, Chaojie Mao, Yulin Pan, Zhen Han, and Jingfeng Zhang. SCEdit: Efficient and controllable image diffusion generation via skip connection editing. In *Proceedings of the IEEE/CVF Conference on Computer Vision and Pattern Recognition (CVPR)*, pages 8995–9004, June 2024. [4](#)
26. Tero Karras, Miika Aittala, Timo Aila, and Samuli Laine. Elucidating the design space of diffusion-based generative models. In Alice H. Oh, Alekh Agarwal, Danielle Belgrave, and Kyunghyun Cho, editors, *Advances in Neural Information Processing Systems*, 2022. [3](#)
27. Zhifeng Kong, Wei Ping, Jiaji Huang, Kexin Zhao, and Bryan Catanzaro. DiffWave: A versatile diffusion model for audio synthesis. *arXiv preprint arXiv:2009.09761*, 2020. [3](#)
28. Black Forest Labs. Flux. <https://github.com/black-forest-labs/flux>, 2024. [10](#)
29. Xingchao Liu, Chengyue Gong, and Qiang Liu. Flow straight and fast: Learning to generate and transfer data with rectified flow. *arXiv preprint arXiv:2209.03003*, 2022. [7](#)
30. Sicheng Mo, Fangzhou Mu, Kuan Heng Lin, Yanli Liu, Bochen Guan, Yin Li, and Bolei Zhou. FreeControl: Training-free spatial control of any text-to-image diffusion model with any condition. In *Proceedings of the IEEE/CVF Conference on Computer Vision and Pattern Recognition (CVPR)*, pages 7465–7475, June 2024. [4](#)
31. Chong Mou, Xintao Wang, Liangbin Xie, Yanze Wu, Jian Zhang, Zhongang Qi, and Ying Shan. T2I-Adapter: Learning adapters to dig out more controllable ability for text-to-image diffusion models. In *AAAI*, volume 38, pages 4296–4304, 2024. [2](#), [4](#)
32. NVIDIA. Cosmos-Transfer1: Conditional world generation with adaptive multi-modal control. *ArXiv*, abs/2503.14492, 2025. [4](#)
33. Alan V. Oppenheim and Jae S. Lim. The importance of phase in signals. *Proceedings of the IEEE*, 69(5):529–541, 1981. [2](#), [5](#), [14](#)
34. Bohao Peng, Jian Wang, Yuechen Zhang, Wenbo Li, Ming-Chang Yang, and Jiaya Jia. ControlNeXt: Powerful and efficient control for image and video generation. *arXiv preprint arXiv:2408.06070*, 2024. [4](#)
35. Vadim Popov, Ivan Vovk, Vladimir Gogoryan, Tasnima Sadekova, and Mikhail Kudinov. Grad-TTS: A diffusion probabilistic model for text-to-speech. In *International Conference on Machine Learning*, pages 8599–8608. PMLR, 2021. [3](#)
36. Michael Psenka, Alejandro Escontrela, Pieter Abbeel, and Yi Ma. Learning a diffusion model policy from rewards via q-score matching. *arXiv preprint arXiv:2312.11752*, 2023. [3](#)
37. Yurui Qian, Qi Cai, Yingwei Pan, Yehao Li, Ting Yao, Qibin Sun, and Tao Mei. Boosting diffusion models with moving average sampling in frequency domain. In *Proceedings of the IEEE/CVF conference on computer vision and pattern recognition*, pages 8911–8920, 2024. [4](#)
38. Alec Radford, Jong Wook Kim, Chris Hallacy, Aditya Ramesh, Gabriel Goh, Sandhini Agarwal, Girish Sastry, Amanda Askell, Pamela Mishkin, Jack Clark, et al.

- Learning transferable visual models from natural language supervision. pages 8748–8763. PmLR, 2021. 10
29. Aditya Ramesh, Prafulla Dhariwal, Alex Nichol, Casey Chu, and Mark Chen. Hierarchical text-conditional image generation with clip latents. *arXiv preprint arXiv:2204.06125*, 2022. 3
 30. Robin Rombach, Andreas Blattmann, Dominik Lorenz, Patrick Esser, and Björn Ommer. High-resolution image synthesis with latent diffusion models. In *CVPR*, pages 10684–10695, June 2022. 10
 31. Daniel L. Ruderman and William Bialek. The statistics of natural images. *Network: Computation in Neural Systems*, 5(4):517–548, 1994. 2
 32. Chitwan Saharia, William Chan, Saurabh Saxena, Lala Li, Jay Whang, Emily Denton, Seyed Kamyar Seyed Ghasemipour, Burcu Karagol Ayan, S Sara Mahdavi, Rapha Gontijo Lopes, et al. Photorealistic text-to-image diffusion models with deep language understanding. *arXiv preprint arXiv:2205.11487*, 2022. 3
 33. Zhenxiong Tan et al. OminiControl2: Efficient conditioning for diffusion transformers. *arXiv preprint arXiv:2503.08280*, 2025. 4
 34. Alibaba Team Wan. Wan: Open and advanced large-scale video generative models. *arXiv preprint arXiv:2503.20314*, 2025. 10
 35. Narek Tumanyan, Michal Geyer, Shai Bagon, and Tali Dekel. Plug-and-play diffusion features for text-driven image-to-image translation. In *Proceedings of the IEEE/CVF Conference on Computer Vision and Pattern Recognition (CVPR)*, pages 1921–1930, June 2023. 10
 36. Julen Urain, Niklas Funk, Jan Peters, and Georgia Chalvatzaki. SE(3)-DiffusionFields: Learning smooth cost functions for joint grasp and motion optimization through diffusion. In *2023 IEEE International Conference on Robotics and Automation (ICRA)*, pages 5923–5930. IEEE, 2023. 3
 37. Zhendong Wang, Jonathan J Hunt, and Mingyuan Zhou. Diffusion policies as an expressive policy class for offline reinforcement learning. *arXiv preprint arXiv:2208.06193*, 2022. 3
 38. Zhou Wang and Eero P. Simoncelli. Translation insensitive image similarity in complex wavelet domain. *IEEE Transactions on Image Processing*, 14(4):466–479, 2005. 2
 39. Wei Wu, Qingnan Fan, Shuai Qin, Hong Gu, Ruoyu Zhao, and Antoni B Chan. Freediff: Progressive frequency truncation for image editing with diffusion models. In *European Conference on Computer Vision*, pages 194–209. Springer, 2024. 4
 40. Runsheng Xu, Hubert Lin, Wonseok Jeon, Hao Feng, Yuliang Zou, Liting Sun, John Gorman, Ekaterina Tolstaya, Sarah Tang, Brandyn White, Ben Sapp, Mingxing Tan, Jyh-Jing Hwang, and Dragomir Anguelov. WOD-E2E: Waymo open dataset for end-to-end driving in challenging long-tail scenarios, 2025. 10
 41. Cuihong Yu, Cheng Han, Chao Zhang, Yuewei Wang, Qihang Hu, Yin Yan, Moran Zhan, Meng Li, and Guangjin Bi. DMFFT: improving the generation quality of diffusion models using fast fourier transform. *Scientific Reports*, 15, March 2025. 4
 42. Jiwen Yu, Yinhuai Wang, Chen Zhao, Bernard Ghanem, and Jian Zhang. FreeDoM: Training-free energy-guided conditional diffusion model. In *Proceedings of the IEEE/CVF International Conference on Computer Vision (ICCV)*, pages 23174–23184, October 2023. 4
 43. Lvmin Zhang, Anyi Rao, and Maneesh Agrawala. Adding conditional control to text-to-image diffusion models. In *ICCV*, pages 3836–3847, 2023. 2, 4
 44. Richard Zhang, Phillip Isola, Alexei A Efros, Eli Shechtman, and Oliver Wang. The unreasonable effectiveness of deep features as a perceptual metric. In *CVPR*, pages 586–595, 2018. 10

45. Siyuan Zhang, Wei Ma, Libin Liu, Zheng Li, and Hongbin Zha. Training-free fourier phase diffusion for style transfer. In *Proceedings of the Thirty-Fourth International Joint Conference on Artificial Intelligence*, pages 2386–2394, 2025. [4](#)
46. Shihao Zhao, Dongdong Chen, Yen-Chun Chen, Jianmin Bao, Shaozhe Hao, Lu Yuan, and Kwan-Yee K. Wong. Uni-ControlNet: All-in-one control to text-to-image diffusion models. In *Advances in Neural Information Processing Systems 36 (NeurIPS)*, 2023. [4](#)